JACS
JOURNAL OF THE AMERICAN CHEMICAL SOCIETY
Article
pubs.acs.org/JACS

# Allosteric Regulation of the Rotational Speed in a Light-Driven Molecular Motor

Adele Faulkner, Thomas van Leeuwen, Ben L. Feringa,* and Sander J. Wezenberg*

Stratingh Institute for Chemistry, University of Groningen, Nijenborgh 4, 9747 AG Groningen, The Netherlands

Supporting Information

**ABSTRACT:** The rotational speed of an overcrowded alkene-based molecular rotary motor, having an integrated 4,5-diazafluorenyl coordination motif, can be regulated allosterically via the binding of metal ions. DFT calculations have been used to predict the relative speed of rotation of three different (i.e., zinc, palladium, and platinum) metal dichloride complexes. The photochemical and thermal isomerization behavior of these complexes has been studied in detail using UV−vis and $^1$H NMR spectroscopy. Our results confirm that metal coordination induces a contraction of the diazafluorenyl lower half, resulting in a reduction of the steric hindrance in the "fjord" region of the molecule, which causes an increase of the rotational speed. Importantly, metal complexation can be accomplished *in situ* and is found to be reversible upon the addition of a competing ligand. Consequently, the rotational behavior of these molecular motors can be dynamically controlled with chemical additives.

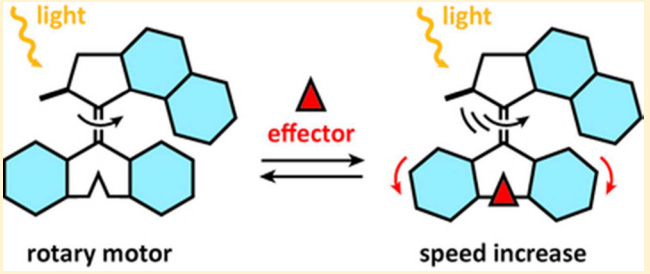


## INTRODUCTION

Various essential biological tasks that involve motion and mechanical work are performed by molecular motor proteins.[1] The activity of these motors is modulated dynamically through complex biological pathways in response to environmental stimuli.[2] Allosteric regulation plays a key role in biological systems in order to switch between active and inactive states. Since allosteric effects involve conformational changes (cf. dynamic motion), the operating principles of allosteric systems are very important in the design of artificial molecular motors and machines.[3,4] Furthermore, allosteric control has been applied to various supramolecular systems to inhibit or activate, for example, catalysis and substrate binding.[5]

Different successful approaches have been taken to develop synthetic motors and machinery that mimic their biological counterparts.[3,4] In this respect, the use of light as the energy source has proven to be particularly attractive for nanotechnology applications.[6−9] However, activity regulation of synthetic nanomotors by multiple external stimuli, as is observed in biological systems,[2] still remains a formidable challenge.

Overcrowded alkene-based rotary motors, developed by our group,[4b,9] are among the most promising candidates to perform work at the nanoscale.[10] They have been applied to control a wide variety of processes, such as self-assembly,[11] substrate binding,[12] wettability,[13] and gel formation.[14] In these motors, repetitive unidirectional rotation is accomplished through sequential photochemical and thermal isomerization steps (Scheme 1A). That is, light excitation can induce a double bond isomerization giving a higher energy (unstable) isomer.[15] This isomer then thermally relaxes to the energetically most favored (stable) isomer via a helix inversion process. In the latter thermal helix inversion (THI) step, the aromatic unit in the upper half of the molecule flips along the lower half. When these photochemical and thermal isomerization steps are repeated, one-half of the motor completes a full 360° rotation with respect to the other half. The THI process is the rate-determining step in the overall rotary cycle and, hence, is what determines the speed of rotation at infinite photon flux.

The development of strategies that allow for regulation of the rotational speed of molecular motors is crucial for bringing nanoscale machinery to a higher level of sophistication and complexity. Within our group, considerable effort has gone into adjusting the frequency of rotation via structural modifications,[16] which required tedious synthetic work. In addition, we have reported on the supramolecular locking of rotation using an acid−base-responsive self-complexing pseudorotaxane,[17] as well as reversing the direction of rotation by base-catalyzed epimerization.[18] Up until now, however, we have not been able to control the speed of rotation in a dynamic way.

Recently, the molecular motor **L1** was developed (see Scheme 1A),[19] which incorporates a 4,5-diazafluorenyl lower half that can bind metal ions. Our initial studies focused on ruthenium bipyridine complex formation with the goal of shifting the excitation wavelength to the visible region, but interestingly, also an effect on the energy barrier for THI was observed. Reversible metal complexation has been applied in the past to control free rotation around a single bond using a "molecular brake" approach as described by the group of

**Received:** June 22, 2016
**Published:** September 26, 2016

  

DOI: 10.1021/jacs.6b06467
J. Am. Chem. Soc. 2016, 138, 13597−13603

**Scheme 1. (A) Isomerization Behavior of Molecular Motor L1 and (B) Rotary Speed Regulation via Reversible Metal Complexation**[a]

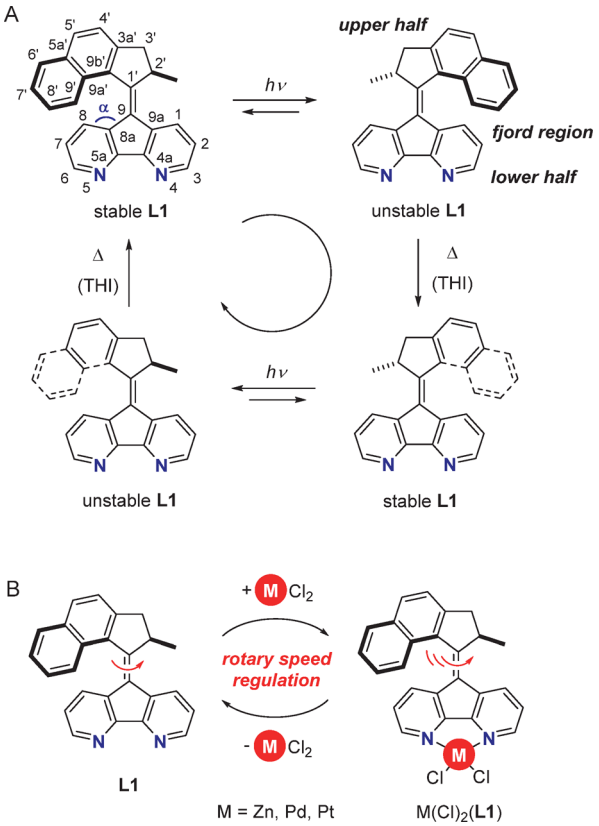


[a]Please note that the two line drawings for stable **L1**, as well as those for unstable **L1**, represent identical molecular structures with different viewpoints.

Kelly.[20] We envisioned that metal complexation to **L1** could also offer an extremely powerful method to postmodify the rotational behavior of light-driven molecular motors in a reversible manner (Scheme 1B).

Herein, we describe the synthesis, characterization, and isomerization behavior of different metal dichloride complexes of **L1**, that is, $Zn(Cl)_2$(**L1**), $Pd(Cl)_2$(**L1**), and $Pt(Cl)_2$(**L1**). Predictions on the relative rates of rotation can be made using DFT optimized molecular structures, which reveal a correlation between the energy barrier for THI and certain structural parameters. We demonstrate that the steric crowding in the "fjord" region, and hence the rotational speed, can be controlled through metal ion binding. Thus, the metal ion can act as a kind of allosteric effector, which induces a structural change. Importantly, the metal complexes can be prepared *in situ* and metal decomplexation occurs upon addition of a competing ligand. This opens up new opportunities to dynamically modulate the properties of light-driven molecular motors and represents a significant step forward toward higher levels of control in nanomechanical devices.

## RESULTS AND DISCUSSION

**DFT Energy Minimizations.** DFT calculations have proven to provide accurate predictions for the structural parameters and the barrier for THI of sterically overcrowded alkene-based molecular motors.[21] It was previously found that the TPSSTPSS functional along with the 6-31G+(d,p):LANL2DZ mixed basis set gives the best approximation of the thermodynamic properties of transition metal complexes.[21,22] Therefore, this method was chosen together with an IEFPCM, $CH_2Cl_2$ solvation model to calculate the structures and relative free energies ($\Delta G$) of the stable and unstable isomers, in addition to the transition states (TS) for THI. The coordination of zinc, palladium, and platinum to 4,5-diazafluorenyl ligands has been studied before and is known to afford stable metal–ligand complexes.[23] For that reason these three metal atoms were initially selected for complexation to **L1**. Furthermore, the resulting metal–ligand complexes are diamagnetic so that $^1$H NMR can be used as a convenient tool to study the photochemical and thermal isomerization processes (*vide infra*).

In the earlier reported X-ray crystal structures of palladium and platinum 4,5-diazafluoren-9-one dichloride complexes, a square planar coordination geometry was observed,[24] whereas the zinc dichloride complex of a structurally related 4,5-diazafluorene derivative revealed a tetrahedral coordination environment.[25] The input geometries for DFT energy minimization were adapted as such, and the obtained molecular structures and relative $\Delta G$ values are presented in Figure 1.

Similar to what has been found for uncomplexed **L1**,[19] the metal–motor complexes exist in a twisted conformation, which is known to be preferred over *anti* folding when the lower half of these structures is sufficiently rigid.[16] Furthermore, inherent to this type of molecular motors,[9b] the methyl group is oriented pseudoaxially in the thermodynamically most stable form and equatorially in the higher energy unstable isomer. The metal-to-nitrogen bond lengths and diazafluorenyl bite angles in the DFT optimized complexes of stable **L1** closely resemble those found in the crystal structures of related metal–ligand complexes.[24,25] The M–N bond lengths in the calculated zinc, palladium, and platinum complexes of the stable ligand are about 2.19, 2.09, and 2.07 Å, respectively (cf. 2.13, 2.08, and 2.06 Å in the reported solid state structures of 4,5-diazafluorene complexes).[24,25] In addition, the observed diazafluorenyl N–M–N bite angles range from 83.2° for zinc and 84.0° for palladium to 83.6° for platinum (cf. 84.8°, 83.7°, and 83.6° in the solid state structures).[24,25]

The TS geometries were searched via a dihedral scan over the central olefinic bond (see the Supporting Information for details). For the palladium and platinum complexes, two different TS structures were found and energy minimized, whereas for the zinc analogue only one TS could be optimized (see Figure 1). The first and lowest energy transition state (TS1) has a planar diazafluorenyl moiety and the C(2′)H and $C(2')CH_3$ protons are located on the same side of the lower half (see Scheme 1 for the atom numbering). The second transition state (TS2), found for $Pd(Cl)_2$(**L1**) and $Pt(Cl)_2$(**L1**), is slightly higher in energy (3–4 kJ mol$^{-1}$) and is structurally similar to that calculated earlier for the uncomplexed ligand **L1**.[19] It has a slightly bent diazafluorenyl lower half with C(2′)H and $C(2')CH_3$ positioned on opposite sides of this unit. The most important structural parameters of all the transition states obtained are summarized in Table 1.

From these structural parameters, it can be derived that metal complexation leads to a contraction of the lower diazafluorenyl half of the molecular motor, which is reflected in the shortened N–N distance and enlarged C(8)–C(8a)–C(9) angle. The angle enlargement implies a reduction of the steric crowding in the "fjord" region. It has been well-established by our group that a decrease of the steric hindrance in this region lowers the


DOI: 10.1021/jacs.6b06467
J. Am. Chem. Soc. 2016, 138, 13597–13603

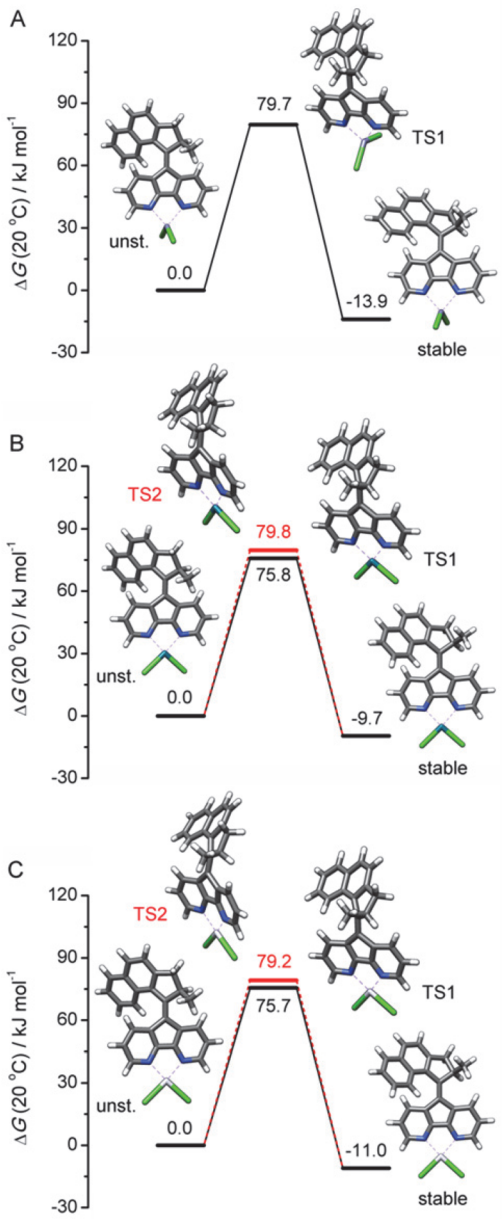


**Figure 1.** Plots of the relative Gibbs free energies (20 °C) between the stable, unstable, and transition state (TS) geometries of (A) $Zn(Cl)_2$(**L1**), (B) $Pd(Cl)_2$(**L1**), and (C) $Pt(Cl)_2$(**L1**) obtained by DFT using the TPSSTPSS/6-31G+(d,p):LANL2DZ level of theory. For the computed data of uncomplexed **L1**, see ref 19.

barrier to THI and hence, enhances the speed of rotation of the motor.[16] Based on these structural features, it is anticipated that the rotary speed of metal-complexed **L1** will increase in the order $Zn(Cl)_2$(**L1**) < $Pd(Cl)_2$(**L1**) < $Pt(Cl)_2$(**L1**). The Gibbs free energy barriers [$\Delta^{\ddagger}G$(20 °C)] for THI, as calculated by DFT (see Figure 1), decrease from zinc to palladium and platinum, which is also expected based on the structural features.

**Synthesis and Isomerization Behavior.** The molecular motor **L1** was obtained by following a recently reported procedure, and it was used as a racemate.[19] Subsequent stirring with $ZnCl_2$ in EtOH at room temperature afforded $Zn(Cl)_2$(**L1**) as a precipitate, which was collected by filtration. Likewise, the addition of **L1** to a solution of $Na_2[PdCl_4]$ in $CH_3OH/CH_2Cl_2$ at room temperature led to precipitation of $Pd(Cl)_2$(**L1**), whereas the corresponding platinum complex $Pt(Cl)_2$(**L1**) was synthesized by heating a solution of **L1** with $K_2[PtCl_4]$ in $H_2O$/MeCN under reflux.

The photochemical and thermal isomerization behavior of the metal-complexed motors was studied in degassed $CH_2Cl_2$ by low temperature UV–vis and $^1$H NMR spectroscopy.[19] In the UV–vis spectrum (Figure 2), the absorption maxima of $Zn(Cl)_2$(**L1**) and $Pd(Cl)_2$(**L1**) are situated around $\lambda$ = 405 nm, whereas $Pt(Cl)_2$(**L1**) has a maximum absorption at $\lambda$ = 422 nm. These maxima are all bathochromically shifted relative to the parent uncomplexed **L1** ($\lambda_{max}$ = 390 nm).[19] Irradiation of the UV–vis samples with 365 nm light at −20 °C resulted in a further bathochromic shift of the major absorption bands to $\lambda$ = 426 nm for $Zn(Cl)_2$(**L1**) and $Pd(Cl)_2$(**L1**) and to $\lambda$ = 431 nm for $Pt(Cl)_2$(**L1**) (see Figure 2). This bathochromic shift is consistent with the formation of the unstable isomer.[9a,16]

Irradiation was continued until no further changes were observed, meaning that the photostationary state (PSS) had been reached. During the course of irradiation, clear isosbestic points were observed indicating that the conversion from stable to unstable isomer is a unimolecular process. Upon warming of the UV–vis samples to room temperature, the original absorption spectra were obtained in all cases, which is consistent with thermal isomerization from the unstable back to the thermodynamically most stable form.[9a,16]

Likewise, $^1$H NMR analysis of solutions in $CD_2Cl_2$, irradiated with 365 nm light at −75 °C, showed a new set of peaks that can be ascribed to the unstable isomer (see Figures S16–S18 in the Supporting Information). By integration of either the C(2′)$CH_3$ or C(3′)CH signals, which are shifted downfield for the photogenerated isomer, the unstable/stable isomer ratios at the PSS were determined (Table 2). Pleasingly, comparison of these $PSS_{365}$ ratios with that of the uncomplexed **L1** reveals that they do not substantially decrease upon metal complexation.[26] When the $^1$H NMR samples were allowed to warm to room temperature, full conversion to the stable isomer was observed. Furthermore, upon the repetition of this irradiation/warming cycle, no degradation products could be detected (Figures S16–S18 in the Supporting Information).

The quantum yields for the photoisomerization process were determined by irradiation of concentrated solutions of the stable isomers in $CH_2Cl_2$. The absorption increase at $\lambda$ = 450 was monitored over time by UV–vis spectroscopy and was

**Table 1. Selected Structural Parameters for the Transitions States of L1 and Its Metal Complexes**[a]

| | | | $Pd(Cl)_2$(**L1**) | | $Pt(Cl)_2$(**L1**) | |
|---|---|---|---|---|---|---|
| | **L1**[19] [TS2] | $Zn(Cl)_2$(**L1**) [TS1] | [TS1] | [TS2] | [TS1] | [TS2] |
| N–N distance (Å) | 3.02 | 2.89 | 2.79 | 2.77 | 2.74 | 2.72 |
| N–M–N bite angle (deg) | | 82.5 | 83.7 | 83.2 | 83.6 | 82.7 |
| C(8)–C(8a)–C(9) angle (deg)[b] | 134.1 | 137.6 | 139.5 | 139.0 | 140.2 | 139.6 |

[a]Calculated by DFT at the TPSSTPSS/6-31G+(d,p):LANL2DZ level of theory. [b]See Scheme 1 for the atom numbering.



DOI: 10.1021/jacs.6b06467
J. Am. Chem. Soc. 2016, 138, 13597–13603

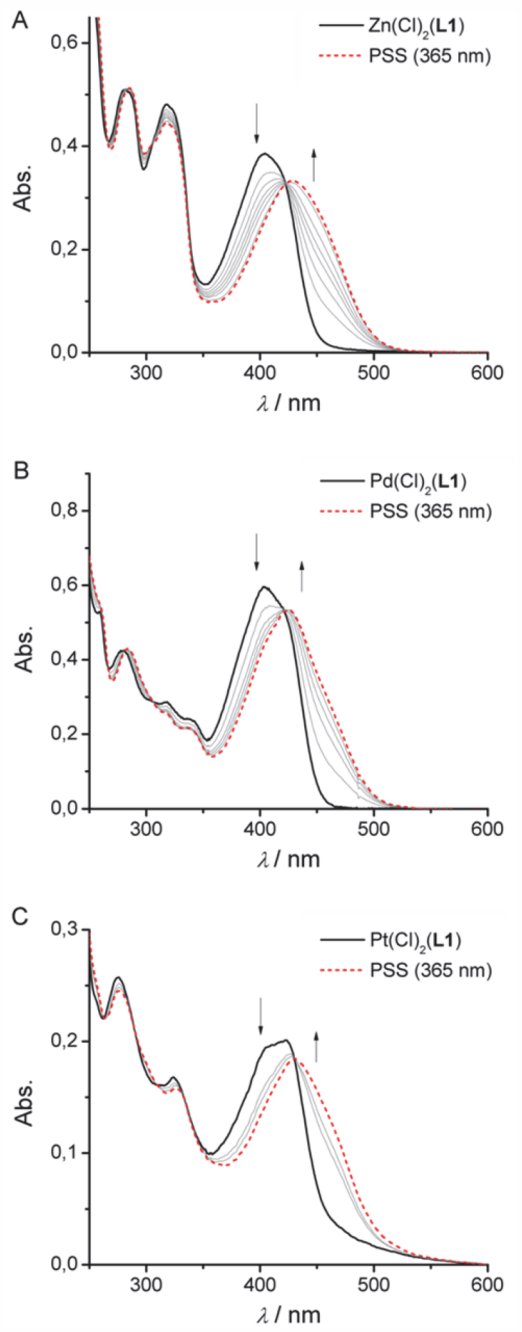


**Figure 2.** UV−vis absorption spectra of (A) $Zn(Cl)_2$(**L1**), (B) $Pd(Cl)_2$(**L1**), and (C) $Pt(Cl)_2$(**L1**) in degassed $CH_2Cl_2$ ($2 \times 10^{-5}$ M) before (solid line) and after (dashed line) irradiation with 365 nm light at −20 °C.

used to calculate the rates of formation of the photogenerated, unstable isomers (see Figures S12−S15 in the Supporting Information). Comparison of these rates to the one measured for the formation of $Fe^{2+}$ ions from ferrioxalate under identical conditions afforded the photochemical quantum yields, which are given in Table 2. These quantum yields range between 3.9% and 6.4% and point out that metal binding has only limited impact on the photoconversion efficiency. Furthermore, the smallest value found for $Pd(Cl)_2$(**L1**) is in line with the lower $PSS_{365}$ ratio, whereas the decreased $PSS_{365}$ ratio for $Pt(Cl)_2$(**L1**) may be ascribed to a higher quantum yield for the "reverse" reaction (i.e., photoconversion from the unstable to the stable isomer).

The rates of the thermal isomerization step were determined over a range of temperatures (−30 to 0 °C, see Figures S8−S11 in the Supporting Information for details) for each of the metal−motor complexes by following the decrease in absorption at $\lambda$ = 450 nm in the UV−vis spectrum. Application of the Eyring equation afforded the thermodynamic parameters (see Figures S8−S10 in the Supporting Information) of which the Gibbs free energies of activation ($\Delta^{\ddagger}G^{\circ}$) are given in Table 2. The corresponding rate constants ($k$) were obtained by extrapolation to 20 °C and used to calculate the half-lives ($t_{1/2}$) at this temperature. Since the THI step is the rate-determining step in the rotary cycle,[9a,16] the rate constant can also be used to define a maximum rotation rate ($\omega$) at 20 °C given infinite photon flux (Table 2). From this data, it is evident that regulation of the rotational speed is possible through metal complexation to **L1**.

The experimentally obtained $\Delta^{\ddagger}G^{\circ}$ values for THI compare well with the DFT calculated ones (see Figure 1). Furthermore, the N−N distances, the C(8)−C(8′)−C(9) angles ($\alpha$, see Table 1), and the experimentally determined $\Delta^{\ddagger}G^{\circ}$ and $k$ values correlate with each other. In agreement with the predictions based on the DFT optimized molecular structures (*vide supra*), the speed of rotation increases in the order: **L1** < $Zn(Cl)_2$(**L1**) < $Pd(Cl)_2$(**L1**) < $Pt(Cl)_2$(**L1**). These results clearly demonstrate that metal coordination induces allosteric changes to the "fjord" region of **L1** and can be used as a convenient tool to regulate the rotational speed. Previous approaches to achieve such changes in the speed of rotation required a new motor design and synthesis.[16] The metal−ligand coordination strategy presented here offers significant benefits over existing methods.

**Reversible Metal Complexation.** When the metal complexes were dissolved in a coordinating solvent (DMSO-$d_6$) or when a strongly coordinating ligand was added (pyridine-$d_5$), the $^1$H NMR spectrum of uncomplexed **L1** was recovered (see Figures S19 and S20 in the Supporting Information). This observation triggered us to investigate the possibility to switch between a metal associated and dissociated state via the addition of chemical stimuli. In that way, the rotary speed of the molecular motor could be reversibly tuned *in situ*, which is important toward the development of more complex molecular motor and machine-like systems.[3,4]

**Table 2. Selected Parameters for the Photochemical and Thermal Isomerization**

| compound | $PSS_{365}$ [unst/stable] | $\phi$ [%] | $\Delta^{\ddagger}G$(20 °C) [kJ mol$^{-1}$] | $k$ (20 °C) [s$^{-1}$] | $t_{1/2}$(20 °C)[a] [s] | $\omega$(20 °C)[b] [Hz] |
|---|---|---|---|---|---|---|
| **L1**[19] | 81:19 | 4.8 | 83.5 | $8.2 \times 10^{-3}$ | 85 | $4.1 \times 10^{-3}$ |
| $Zn(Cl)_2$(**L1**) | 78:22 | 5.7 | 81.5 | $1.8 \times 10^{-2}$ | 38 | $9.0 \times 10^{-3}$ |
| $Pd(Cl)_2$(**L1**) | 67:33 | 3.9 | 78.2 | $7.0 \times 10^{-2}$ | 9.8 | $3.5 \times 10^{-2}$ |
| $Pt(Cl)_2$(**L1**) | 75:25 | 6.4 | 75.1 | 0.25 | 2.7 | 0.13 |

[a]Half-life, $t_{1/2}^{\circ} = \ln(2)/k_{\Delta}^{\circ}$. [b]Maximum rotation rate, $\omega^{\circ} = 1/2k_{\Delta}^{\circ}$.



DOI: 10.1021/jacs.6b06467
J. Am. Chem. Soc. 2016, 138, 13597−13603

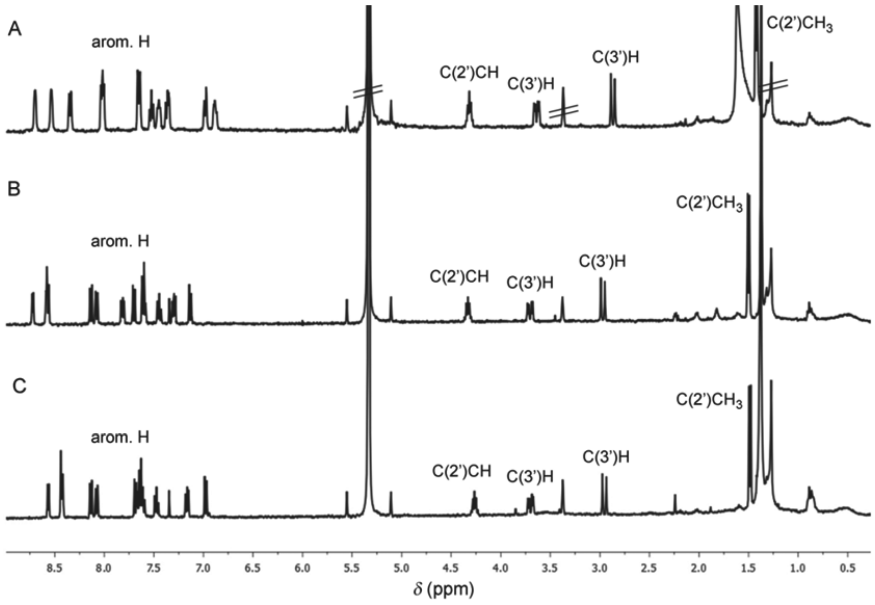


**Figure 3.** (A) $^1$H NMR spectrum of **L1** ($2 \times 10^{-3}$ M solution in $CD_2Cl_2/CD_3OD$) and $^1$H NMR spectrum after (B) the addition of either $ZnCl_2$ to the solution of **L1**, which generates $Zn(Cl)_2$(**L1**), or (C) the addition of $Na_2[PdCl_4]$ to **L1**, which generates $Pd(Cl)_2$(**L1**).

The *in situ* metal complex formation and metal decomplexation were studied by $^1$H NMR and UV−vis spectroscopy. Zinc and palladium were used because the corresponding metal−motor complexes are formed at room temperature. Addition of $ZnCl_2$ or $Na_2[PdCl_4]$ to ligand **L1** dissolved in $CD_2Cl_2/CD_3OD$ afforded $^1$H NMR spectra consistent with those of the previously isolated $Zn(Cl)_2$(**L1**) and $Pd(Cl)_2$(**L1**) complexes (Figure 3). Subsequent addition of pyridine-$d_5$ induced metal decomplexation as evidenced by the regeneration of the $^1$H NMR spectrum of **L1** (see Figures S21 and S22 in the Supporting Information).

During these $^1$H NMR experiments significant color changes were observed upon addition of the metal salts, which prompted us to additionally monitor this *in situ* reversible complexation by UV−vis spectroscopy. Adding either $ZnCl_2$ or $Na_2[PdCl_4]$ to a solution of **L1** in $CH_2Cl_2/CH_3OH$ resulted in the bathochromic shifting of the absorption maxima, which is consistent with formation of the metal complex (Figure 4). Again, metal dissociation was successfully achieved through the addition of pyridine as is clear from the hypsochromic shift back to the original absorption maximum. In the case of zinc, these metal complexation and decomplexation steps were repeated multiple times (see Figure S23 in the Supporting Information). Hence, these combined $^1$H NMR and UV−vis experiments reveal that dynamic regulation of the rotation rate is feasible via addition of chemical stimuli.

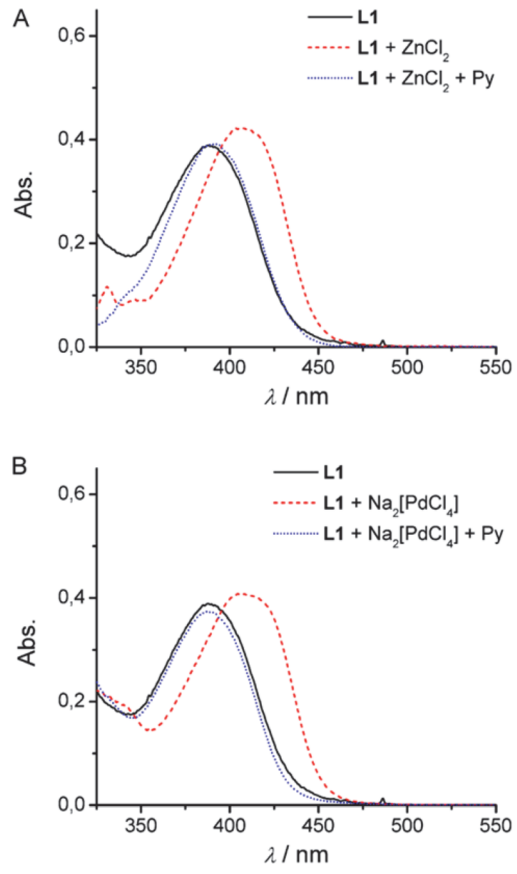


**Figure 4.** UV−vis spectrum of **L1** ($2 \times 10^{-5}$ M in $CH_2Cl_2/CH_3OH$, 40:1, solid line) upon addition of either (A) $ZnCl_2$ or (B) $Na_2[PdCl_4]$ (dashed line) followed by the addition of pyridine (dotted line).

## CONCLUSIONS

In conclusion, we have presented the synthesis and characterization of zinc, palladium, and platinum dichloride complexes of molecular motor **L1**. The photochemical and thermal isomerization behavior of these metal−motor complexes has been studied in detail. Interestingly, the speed of rotation of molecular motor **L1** increases through metal complexation in the order $Zn(Cl)_2$(**L1**) < $Pd(Cl)_2$(**L1**) < $Pt(Cl)_2$(**L1**), which is in agreement with predictions based on DFT geometry optimization. Binding of metal ions to **L1** leads to a contraction of the 4,5-diazafluorenyl lower half and the simultaneous reduction of the steric crowding in the "fjord" region. Hence, the metal ion can be regarded as an allosteric effector. Furthermore, the metal−motor complexes can be generated *in situ*, and the addition of a competitive ligand causes full metal decomplexation. Consequently, the rotational behavior of these


DOI: 10.1021/jacs.6b06467
J. Am. Chem. Soc. 2016, 138, 13597−13603

motors can be tuned reversibly in a highly practical and versatile manner with a level of control that is unprecedented. Therefore, this work represents a critical step forward to integrated chemical regulation in molecular machines that are operated by light. Other applications are foreseen in photoswitchable transition metal catalysis, surface anchoring, and molecular sensing.

## ■ ASSOCIATED CONTENT

### Supporting Information

The Supporting Information is available free of charge on the ACS Publications website at DOI: 10.1021/jacs.6b06467.

Experimental procedures, $^{1}H$ and $^{13}C$ NMR spectra of title compounds, UV−vis spectra upon irradiation and Eyring plot analysis, quantum yield determination, PSS determination and reversible complexation studies by $^{1}H$ NMR, and theoretical calculations (PDF)

## ■ AUTHOR INFORMATION


### Corresponding Authors

*b.l.feringa@rug.nl

*s.j.wezenberg@rug.nl


### Notes

The authors declare no competing financial interest.

## ■ ACKNOWLEDGMENTS

This work was financially supported by The Netherlands Organization for Scientific Research (NWO-CW, Veni Grant No. 722.014.006 to S.J.W.), the Ministry of Education, Culture and Science (Gravitation Program No. 024.001.035), the Leverhulme Trust (Study Abroad Studentship to A.F.), and the European Research Council (Advanced Investigator Grant, No. 227897 to B.L.F.). We thank Michael M. Lerch for help with quantum yield determinations.

## ■ REFERENCES


(1) Schliwa, M. *Molecular Motors*; Wiley-VCH: Weinheim, Germany, 2003.

(2) Mallik, R.; Gross, S. P. *Curr. Biol.* **2004**, *14*, R971−R982.

(3) For selected reviews, see: (a) Balzani, V.; Credi, A.; Raymo, F. M.; Stoddart, J. F. *Angew. Chem., Int. Ed.* **2000**, *39*, 3348−3397. (b) Balzani, V.; Credi, A.; Venturi, M. *Molecular Devices and Machines − A Journey into the Nano World*; Wiley-VCH: Weinheim, Germany, 2003. (c) Kinbara, K.; Aida, T. *Chem. Rev.* **2005**, *105*, 1377−1400. (d) Browne, W. R.; Feringa, B. L. *Nat. Nanotechnol.* **2006**, *1*, 25−35. (e) Champin, B.; Mobian, P.; Sauvage, J.-P. *Chem. Soc. Rev.* **2007**, *36*, 358−366. (f) Kay, E. R.; Leigh, D. A.; Zerbetto, F. *Angew. Chem., Int. Ed.* **2007**, *46*, 72−191. (g) Coskun, A.; Banaszak, M.; Astumian, R. D.; Stoddart, J. F.; Grzybowski, B. A. *Chem. Soc. Rev.* **2012**, *41*, 19−30. (h) Bruns, C. J.; Stoddart, J. F. *Acc. Chem. Res.* **2014**, *47*, 2186−2199. (i) Credi, A.; Silvi, S.; Venturi, M. *Top. Curr. Chem.* **2014**, *354*, 1−34. (j) Erbas-Cakmak, S.; Leigh, D. A.; McTernan, C. T.; Nussbaumer, A. L. *Chem. Rev.* **2015**, *115*, 10081−10206. (k) Kay, E. R.; Leigh, D. A. *Angew. Chem., Int. Ed.* **2015**, *54*, 10080−10088. (l) Abendroth, J. M.; Bushuyev, O. S.; Weiss, P. S.; Barrett, C. J. *ACS Nano* **2015**, *9*, 7746−7768. (m) Peplow, M. *Nature* **2015**, *525*, 18−21.

(4) For selected examples, see: (a) Kelly, T. R.; De Silva, H.; Silva, R. A. *Nature* **1999**, *401*, 150−152. (b) Koumura, N.; Zijlstra, R. W. J.; van Delden, R. A.; Harada, N.; Feringa, B. L. *Nature* **1999**, *401*, 152−155. (c) Leigh, D. A.; Wong, J. K. Y.; Dehez, F.; Zerbetto, F. *Nature* **2003**, *424*, 174−179. (d) Badjic, J. D.; Balzani, V.; Credi, A.; Silvi, S.; Stoddart, J. F. *Science* **2004**, *303*, 1845−1849. (e) Hernández, J. V.; Kay, E. R.; Leigh, D. A. *Science* **2004**, *306*, 1532−1537. (f) Fletcher, S. P.; Dumur, F.; Pollard, M. M.; Feringa, B. L. *Science* **2005**, *310*, 80−82. (g) Wilson, M. R.; Solá, J.; Carlone, A.; Goldup, S. M.; Lebrasseur, N.; Leigh, D. A. *Nature* **2016**, *534*, 235−240. (h) Collins, B. S. L.; Kistemaker, J. C. M.; Otten, E.; Feringa, B. L. *Nat. Chem.* **2016**, *8*, 860−866.

(5) (a) Takeuchi, M.; Ikeda, M.; Sugasaki, A.; Shinkai, S. *Acc. Chem. Res.* **2001**, *34*, 865−873. (b) Kovbasyuk, L.; Krämer, R. *Chem. Rev.* **2004**, *104*, 3161−3188. (c) Oliveri, C. G.; Ulmann, P. A.; Wiester, M. J.; Mirkin, C. A. *Acc. Chem. Res.* **2008**, *41*, 1618−1629. (d) Wiester, M. J.; Ulmann, P. A.; Mirkin, C. A. *Angew. Chem., Int. Ed.* **2011**, *50*, 114−137.

(6) For reviews, see: (a) Saha, S.; Stoddart, J. F. *Chem. Soc. Rev.* **2007**, *36*, 77−92. (b) Katsonis, N.; Lubomska, M.; Pollard, M. M.; Feringa, B. L.; Rudolf, P. *Prog. Surf. Sci.* **2007**, *82*, 407−434. (c) Ceroni, P.; Credi, A.; Venturi, M.; Balzani, V. *Photochem. Photobiol. Sci.* **2010**, *9*, 1561−1573.

(7) For molecular tweezers, see: (a) Shinkai, S.; Nakaji, T.; Ogawa, T.; Shigematsu, K.; Manabe, O. *J. Am. Chem. Soc.* **1981**, *103*, 111−115. (b) Muraoka, T.; Kinbara, K.; Kobayashi, Y.; Aida, T. *J. Am. Chem. Soc.* **2003**, *125*, 5612−5613. (c) Muraoka, T.; Kinbara, K.; Aida, T. *Nature* **2006**, *440*, 512−515.

(8) For rotaxane shuttles, see: (a) Benniston, A. C.; Harriman, A. *Angew. Chem., Int. Ed. Engl.* **1993**, *32*, 1459−1461. (b) Murakami, H.; Kawabuchi, A.; Kotoo, K.; Kunitake, M.; Nakashima, N. *J. Am. Chem. Soc.* **1997**, *119*, 7605−7606. (c) Coskun, A.; Friedman, D. C.; Li, H.; Patel, K.; Khatib, H. A.; Stoddart, J. F. *J. Am. Chem. Soc.* **2009**, *131*, 2493−2495. (d) Bottari, G.; Leigh, D. A.; Pérez, E. M. *J. Am. Chem. Soc.* **2003**, *125*, 13360−13361. (e) Li, H.; Fahrenbach, A. C.; Coskun, A.; Zhu, Z.; Barin, G.; Zhao, Y.; Botros, Y. Y.; Sauvage, J.-P.; Stoddart, J. F. *Angew. Chem., Int. Ed.* **2011**, *50*, 6782−6788.

(9) For rotary motors, see: (a) Koumura, N.; Geertsema, E. M.; van Gelder, M. B.; Meetsma, A.; Feringa, B. L. *J. Am. Chem. Soc.* **2002**, *124*, 5037−5051. (b) Feringa, B. L. *J. Org. Chem.* **2007**, *72*, 6635−6652. (c) Greb, L.; Lehn, J.-M. *J. Am. Chem. Soc.* **2014**, *136*, 13114−13117. (d) Guentner, M.; Schildhauer, M.; Thumser, S.; Mayer, P.; Stephenson, D.; Mayer, P. J.; Dube, H. *Nat. Commun.* **2015**, *6*, 8406.

(10) (a) Eelkema, R.; Pollard, M. M.; Vicario, J.; Katsonis, N.; Ramon, B. S.; Bastiaansen, C. W. M.; Broer, D. J.; Feringa, B. L. *Nature* **2006**, *440*, 163−163. (b) van Delden, R. A.; ter Wiel, M. K. J.; Pollard, M. M.; Vicario, J.; Koumura, N.; Feringa, B. L. *Nature* **2005**, *437*, 1337−1340.

(11) van Dijken, D. J.; Chen, J.; Stuart, M. C. A.; Hou, L.; Feringa, B. L. *J. Am. Chem. Soc.* **2016**, *138*, 660−669.

(12) (a) Wezenberg, S. J.; Vlatković, M.; Kistemaker, J. C. M.; Feringa, B. L. *J. Am. Chem. Soc.* **2014**, *136*, 16784−16787. (b) Vlatković, M.; Feringa, B. L.; Wezenberg, S. J. *Angew. Chem., Int. Ed.* **2016**, *55*, 1001−1004.

(13) Chen, K.-Y.; Ivashenko, O.; Carroll, G. T.; Robertus, J.; Kistemaker, J. C. M.; London, G.; Browne, W. R.; Rudolf, P.; Feringa, B. L. *J. Am. Chem. Soc.* **2014**, *136*, 3219−3224.

(14) (a) Li, Q.; Fuks, G.; Moulin, E.; Maaloum, M.; Rawiso, M.; Kulic, I.; Foy, J. T.; Giuseppone, N. *Nat. Nanotechnol.* **2015**, *10*, 161−165. (b) Wezenberg, S. J.; Croisetu, C. M.; Stuart, M. C. A.; Feringa, B. L. *Chem. Sci.* **2016**, *7*, 4341−4346.

(15) The term unstable refers to a higher-energy, metastable state and is not related to the chemical stability.

(16) (a) Vicario, J.; Meetsma, A.; Feringa, B. L. *Chem. Commun.* **2005**, *116*, 5910−5912. (b) Vicario, J.; Walko, M.; Meetsma, A.; Feringa, B. L. *J. Am. Chem. Soc.* **2006**, *128*, 5127−5135.

(17) Qu, D.-H.; Feringa, B. L. *Angew. Chem., Int. Ed.* **2010**, *49*, 1107−1110.

(18) Ruangsupapichat, N.; Pollard, M. M.; Harutyunyan, S.; Feringa, B. L. *Nat. Chem.* **2011**, *3*, 53−60.

(19) Wezenberg, S. J.; Chen, K.-Y.; Feringa, B. L. *Angew. Chem., Int. Ed.* **2015**, *54*, 11457−11461.

(20) Kelly, T. R.; Bowyer, M. C.; Bhaskar, K. V.; Bebbington, D.; Garcia, A.; Lang, F.; Kim, M. H.; Jette, M. P. *J. Am. Chem. Soc.* **1994**, *116*, 3657−3658.

(21) (a) Klok, M.; Walko, M.; Geertsema, E. M.; Ruangsupapichat, N.; Kistemaker, J. C. M.; Meetsma, A.; Feringa, B. L. *Chem. - Eur. J.*

**2008**, *14*, 11183−11193. (b) Kazaryan, A.; Kistemaker, J. C. M.; Schäfer, L. V.; Browne, W. R.; Feringa, B. L.; Filatov, M. *J. Phys. Chem. A* **2010**, *114*, 5058−5067. (c) Pérez-Hernández, G.; González, L. *Phys. Chem. Chem. Phys.* **2010**, *12*, 12279−12289. (d) Oruganti, B.; Fang, C.; Durbeej, B. *Phys. Chem. Chem. Phys.* **2015**, *17*, 21740−21751.

(22) Yang, Y.; Weaver, M. N.; Merz, K. M., Jr. *J. Phys. Chem. A* **2009**, *113*, 9843−9851.

(23) For the synthesis of diazafluorenyl Zn, Pd, and Pt complexes, see: (a) Baysal, A.; Connor, J. A.; Wallis, J. D. *J. Coord. Chem.* **2001**, *53*, 347−354. (b) Lu, G.; Ho, C.; Wang, Q.; Wong, W.; Chui, C.; Wong, R. S.; Gambari, R.; Lau, F.; Yuen, M. C.; Tong, C. S.; Chan, A. K.; Tang, J. C.; Ho, K.; Cheng, G. Y. *Aust. J. Chem.* **2008**, *61*, 975−980.

(24) (a) Xu, Z.-G.; Liu, H.-Y.; Zhan, Q.-G.; Chen, J.; Xu, M.-J. *Acta Crystallogr., Sect. E: Struct. Rep. Online* **2009**, *E65*, m1166. (b) Biju, A. R.; Rajasekharan, M. V.; Bhat, S. S.; Khan, A. A.; Kumbhar, A. S. *Inorg. Chim. Acta* **2014**, *423*, 93−97.

(25) Zhu, Q.-Y.; Yu, L.; Qin, Y.-R.; Huo, L.-B.; Shao, M.-Y.; Dai. *CrystEngComm* **2011**, *13*, 2521−2528.

(26) Please note that a decrease in PSS ratio is actually not a limitation for these molecular motors since the succeeding THI step is a "forward" process in the rotary cycle.



DOI: 10.1021/jacs.6b06467
*J. Am. Chem. Soc.* 2016, 138, 13597−13603